Microsystem Technologies (2020) 26:183–193
https://doi.org/10.1007/s00542-019-04540-x

TECHNICAL PAPER

Advanced numerical analysis for vibration characteristics and ride comfort of ultra-high-speed maglev train

Hue Ha[1] · Jungwan Park[2] · Kyoung-Su Park[1]

Received: 3 December 2018 / Accepted: 5 July 2019 / Published online: 7 August 2019

Abstract
Magnetic levitation (maglev) trains are environmentally-friendly, require little maintenance, and allow for mass transportation. For these reasons, the demand for ultra-high-speed maglev trains has been increasing. Maglev trains can be classified with two suspension types, electro dynamic suspension (EDS) and electromagnetic suspension (EMS). EDS-type trains are suitable for ultra-high-speed because levitation suspension gap is over 100 mm compared with levitation suspension gap of 10 mm for EMS. When speed goes faster, it is hard to control the small suspension gap rapidly in EMS type. To analyze the EDS-type maglev train, electromagnetic forces were calculated with the superconducting coils and magnets using 2D analytical model. Based on the calculated forces, the lookup tables for the levitation and guidance force were employed in the total couple-fielded analysis. Ultra-high-speed maglev train was simulated by using the ADAMS multi-body dynamic program. The simulation was carried out with two car body models, rigid and flexible car body. In order to construct flexible car bodies with the modal information, the finite element method was used and they were constructed with the equivalent elements using ANSYS^{TM}. The final framework was constructed in MATLAB Simulink, and we co-simulated the dynamics and the electromagnetics with the constructed simulation frame work. To consider disturbances caused by irregularities, random and power spectral density (PSD) were used to analyze the vibrational interaction. As results, the ride comforts for PSD were a little bit worse than the results for random irregularity because the characteristics of PSD irregularity have more low excitation frequencies. The use of PSD inputs and flexible car body models need to be considered to improve the simulation accuracy.

1 Introduction

Magnetic levitation (maglev) trains are environmentally-friendly, require little maintenance, have a compact design, and allow for mass transportation (Lee et al. 2006). Accordingly, these trains have attracted a great deal of attention (Tsuruga 1992; Fujie 1999; Fujimoto et al. 2000; Miyamoto et al. 2004). In the maglev trains, levitation is critical, and is of two types: superconductive maglev electromagnetic suspension (EMS) and electro dynamic suspension (EDS). For levitation, EMS system uses electromagnetic attraction force as its suspending force, while the EDS system uses magnetic repulsive force. For these reasons, EMS system uses the very low suspension gap (under 10 mm) and the EDS system can remain a larger suspension gap (up to 100 mm). Therefore, EDS system has very little risk to contact between the ground and bogies because of large suspension gap and it is unnecessary to control the air gap between the vehicle and the track during the operation. As a result, this system is suitable for long-distance and high-speed transport compared to EMS which has to control the gap continuously during the operation. Because of these reasons, the demand for EDS-type trains have been preferred to EMS-type trains (Lee et al. 2006; Yaghoubi and Ziari 2010; Ahmed et al. 2014) in ultra-high-speed trains.

From a vibration and a ride comfort, aerodynamics can affect vibrations of bogie and car body gap. Also, irregularities in propulsion, levitation, and guidance (PLG) coils and superconducting (SC) coils promote vibration, compromising stability and ride comfort. When constructing PLG coils on the panel, there are some difficulty in

✉ Kyoung-Su Park
pks6348@gachon.ac.kr

[1] Department of Mechanical Engineering, Gachon University, 1342 Seongnamdaero, Sujeong-gu, Seongnam-si, Gyeonggi-do 461-701, Korea

[2] Hyundai Motor, 150, Hyundaiyeonguso-ro, Namyang-eup, Hwaseong-si, Gyeonggi-do, Republic of Korea

constructions. For example, guideway which PLG coils are installed, can be elongated and shrunk because of the temperature (Seki et al. 1996). Also, guideway panels have random imperfections, these imperfections induce the resonance of the maglev system (Ohsaki et al. 2000; Early et al. 2002). These imperfection affects the electromagnetic force system which consists of PLG and SC coils. As a result, the electromagnetic forces are changed by these imperfections. In our simulation, we inputted the displacement irregularity which corresponds to these imperfections. Because of these characteristics, vibration analyses of real-world trains were desirable (Seki et al. 1996; Kim et al. 2002). However, such trains costs about $44.7 billion (Rose et al. 2008), and analysis was very time-consuming. Depending on the point of view, numerical simulation features two car body modeling methods; car bodies are regarded as rigid or flexible. Rigid models were preferred for simplicity (Ohsaki et al. 2000; Song and Fujino 2008; Suzuki et al. 2008); even though the flexible models are complex and the computing costs high, it was preferred for the accuracy. Rigid models analyze a simple stability at low speed. Flexible models can evaluate stability and ride comfort in the real world (Zhang et al. 2013) better. Flexible models feature vibrational modes, greatly complicating simulations given the lack of relevant real-world data. Flexible models incorporate detailed vibrational modes; rigid models exploit only vertical and rolling modes; the flexible models are more accurate (Diana et al. 2002; Tomioka et al. 2003; Ohsaki and Bando 2006; Zhou et al. 2009; Zhang et al. 2013). Diana et al. (2002) and Tomioka et al. (2003) used a flexible model to analyze real trains. Zhou et al. (2009) and Zhang et al. (2013) compared single-car flexible and rigid models. However, only the middle car body was considered, and the models featured simple beams (Ohsaki and Bando 2006) Therefore, the detailed dynamics of the 1st and 3rd car bodies were not considered.

In this paper, electromagnetic forces were calculated with the 3D-full SC coils and magnets by using ANSYS Maxwell. After that, the model was simplified in two degree of freedom (DOF) and verified with the 3D-full model (Kim et al. 2018). Based on the calculation of the force, we employed lookup tables for levitation and guidance forces. Propulsion was modeled as a constant velocity of 500 km/h (138 m/s). We modeled an ultra-high-speed maglev train using the ADAMS multi-body dynamic program. The initial rigid body models featured three car bodies and four bogies for simplicity. We then derived flexible car bodies using a commercial finite-element program (ANSYS). The final framework was constructed in MATLAB Simulink, and the dynamics and the electromagnetics were co-simulated with the constructed framework. Both random irregularity and power spectral density (PSD) were used to analyze the vibrational characteristics of an ultra-high-speed maglev train. We compared random signal inputs with PSDs, greatly enhancing accuracy (Guangwei et al. 2007), and analyzed the vibrational interaction between car body and ride comfort.

2 Dynamic modeling of a maglev train

2.1 Numerical simulation

The maglev train parameters were based on those of the real-world Yamanashi test line. The length of the 1st and 3rd car body was 28 m, and that of the 2nd car body was 24.3 m; the width and height of all three car bodies were 2.9 and 3.27 m, respectively (Shirakuni et al. 2002). The 1st and 4th bogies were non-articulated; the 2nd and 3rd were articulated. The 2nd bogie was connected to the 1st and 2nd car body; the 3rd bogie was connected to the 2nd and 3rd car body (Hoshino et al. 2012). The bogie length was 5.4 m, the width was 3.15 m and the height was 1.23 m (Yamamoto et al. 2004; Hoshino et al. 2008). The use of three car bodies and four bogies allows consideration of the articulated bogie effect. All bogies were made of rigid model. The car bodies and bogies were connected via four springs (0.38 MN/m), four dampers (10 kNs/m), and four translation joints. We did not consider lateral or yaw dampers in our simulation. The car bodies were connected using spherical joints to allow consideration of rotation motion of car body. Figure 1 shows the rigid and flexible models. In Fig. 1a, the train car body is made of rigid body model, which doesn't have flexible modal information. On the other hand, the train car body is made of flexible body model, which contains flexible mode information. In Fig. 1b. For the reference, Fig. 1c included SC coils and PLG coils. SC coil is originally located on the side of the bogie like red box in the figure. PLG coils, which shaped like "8" were located on the wall of the panel. To know the forces between the two coils, ANSYS Maxwell program was used and the levitation and guidance force was based on the following equation [see Eq. (1)].

$$F_\alpha = -i_{sc} i_g \frac{\partial M}{\partial \alpha} \tag{1}$$

To describe to equation F_α is the force of levitation and guidance force, i_{sc} means the current of the superconducting coil, i_g means the current in guideway and $\frac{\partial M}{\partial \alpha}$ is the mutual inductance between the two coils. According to the equation, forces were calculated. To apply to multi-body dynamic simulation, SC and PLG coils relation transferred to forces.

We used a finite element method (FEM) to consider the characteristics of a flexible car body. Figure 2a shows the

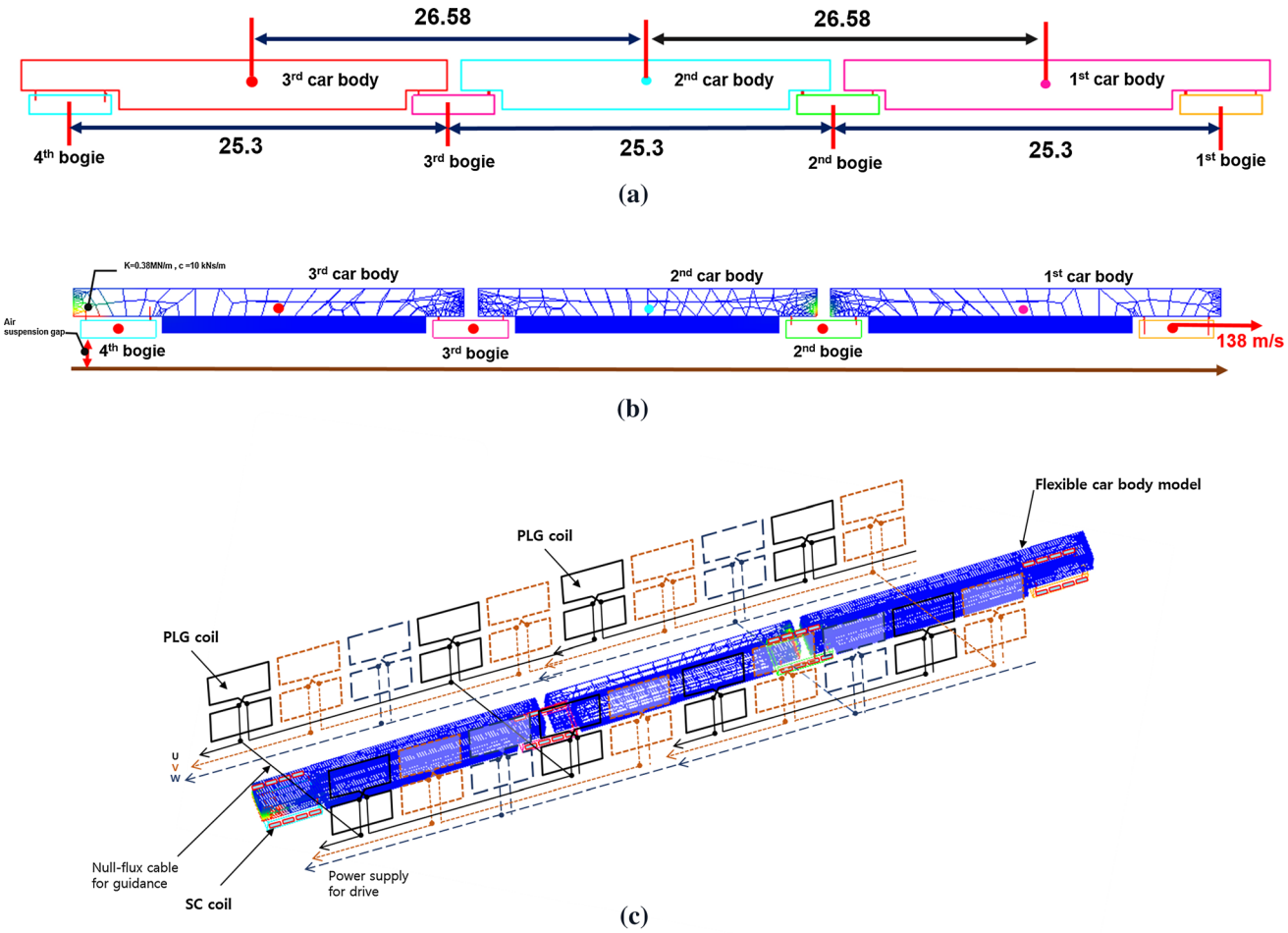

Fig. 1 Simulation models of **a** a rigid car body and **b** a flexible car body **c** side view of the maglev system

flexible car body modeling using FEM method. The body consists of a roof, a floor, a bottom, and walls. Although real-world layers are constructed as frames, we assumed that all layers have an equivalent thickness to simplify the simulation.

The car body was made of mild steel with a Young's modulus of 200 GPa, Poisson ratio of 0.3, and density of 7700 kg/m^3. The weight and thickness of the 1st and 3rd bodies differed from those of the 2nd car body. To construct the simulation model, we referred to a practical Shinkansen L0 model. According to the Yamanashi test line, the 1st and 3rd car bodies weigh 32 tons and the 2nd car body weighs 23 tons. 1st and 3rd car body is for crew cabin and power source room on the other hand, 2nd car body is for passengers (Shirakuni et al. 2002). Because of the power source room 1st and 3rd car body weighs more than 2nd car body. Choosing the dimensions of thickness are to verify (Tomioka et al. 2003) with 1st, 2nd, 3rd mode frequencies (10.15 Hz, 15.44 Hz, 18.81 Hz). In this system to verify the frequency, equivalent thickness has been used. The 1st and 3rd car bodies (2nd car body) had a roof thickness of 0.008 m (0.008 m). The floor thickness was 0.016 m (0.011 m) and the bottom thickness was 0.016 m (0.011 m). The wall thickness was 0.008 m (0.006 m). The 1st and 3rd car body models contained 7719 elements; the 2nd car body model had 9693 elements to allow more detailed consideration of its dynamic characteristics. Twenty mode characteristics were considered. The flexible models were built using commercial ANSYS software and the models were saved as modal neutral files (MNFs). First, modeling was performed using the FEM. After modeling in order to connect with ADAMS software nodes of the modeling should be selected. In Fig. 2b, slave nodes have to be selected to connect with the master node. Then, pick the master node to connect the slave nodes. These master node gets to connect with the ADAMS springs or joints. Master nodes are for rigid body element (RBE2), which are connected to the springs or joints.

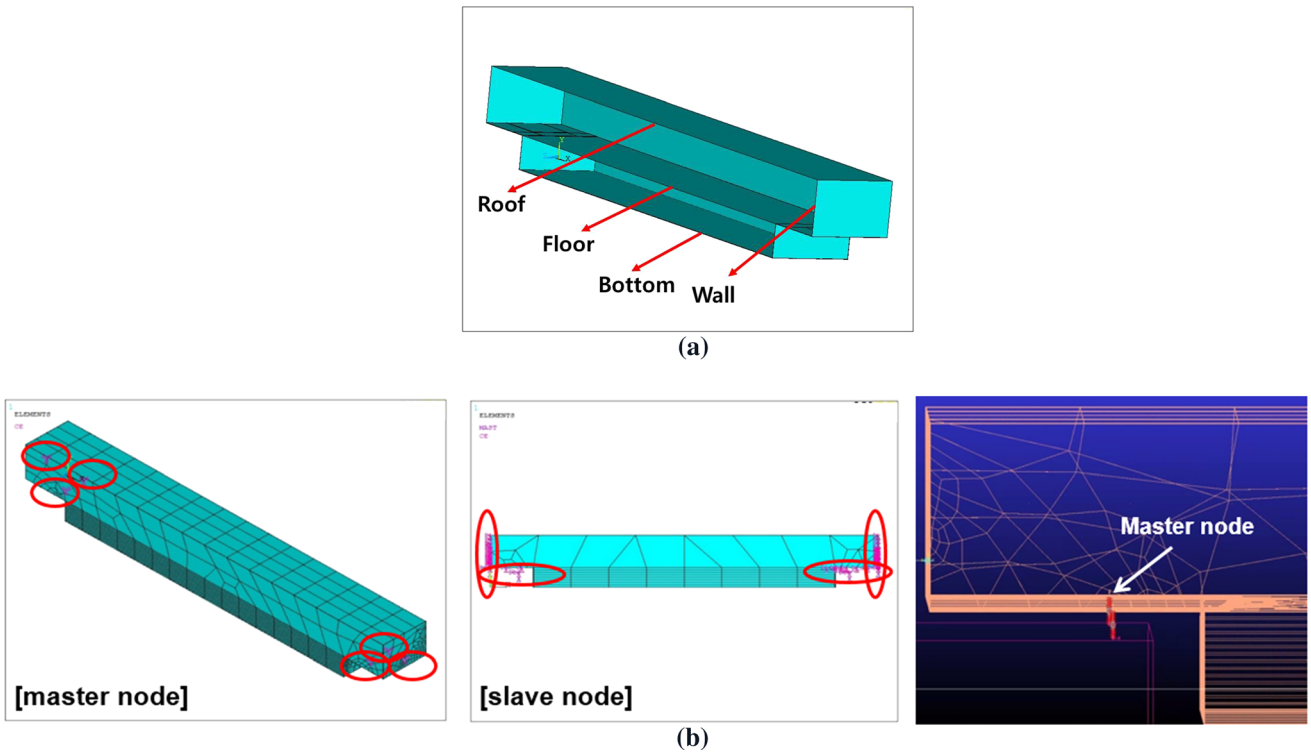

Fig. 2 **a** Modeling of flexible car body, **b** master nodes and slave nodes of the modeling

Forces were calculated using ANSYS Maxwell software. Simulation featured two-dimensional SC and PLG coils (Yonezu et al. 2017). Figure 3 shows the forces acting on each PLG coil, as calculated by Kim et al. (2018); the levitation force occurs in perpendicular direction and guidance force occurs in parallel direction. The calculation forces were in excellent agreement with the experimental data of Tanaka et al. (2007). Therefore, this simulation used the results as levitation and guidance forces below. Propulsion force gets affected by variety of parameters. For example, aerodynamic effect affects the force. It is difficult to consider the effects of those parameters so to simplify the parameters. We have assumed the effect as constant velocity.

2.2 Disturbances caused by irregularities

To analyze a vehicle response and evaluate a ride comfort, disturbances caused by irregularities must be considered (Zhou et al. 2009; Zhao et al. 2010; Shi et al. 2014). Mostly, irregularities occur according to imperfection of the coil and the magnet (Seki et al. 1996) such as misalignments as mentioned above. These kinds of disturbance can induce resonances due to periodic imperfections (Early et al. 2002). To consider the irregularities, irregularities were added to the vertical displacement of the

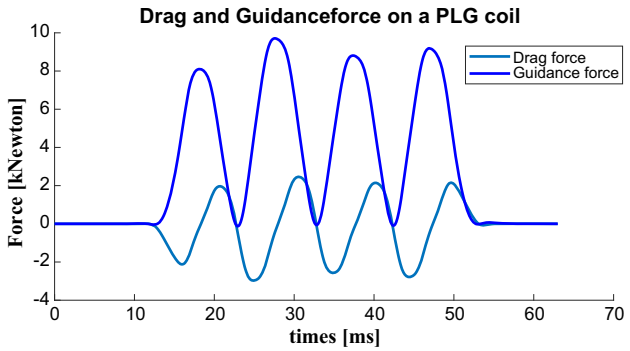

Fig. 3 The calculated levitation and guidance forces of Kim et al. (2018)

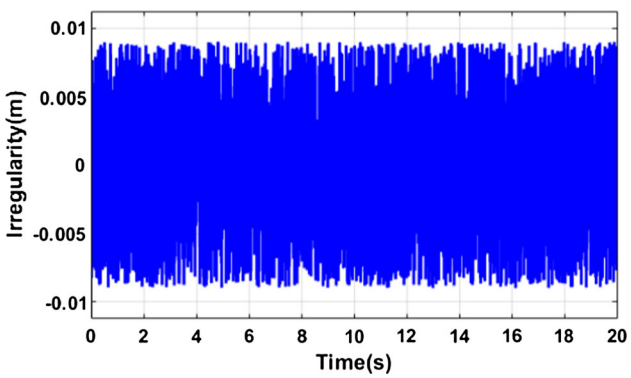

Fig. 4 Irregularities caused by random signaling

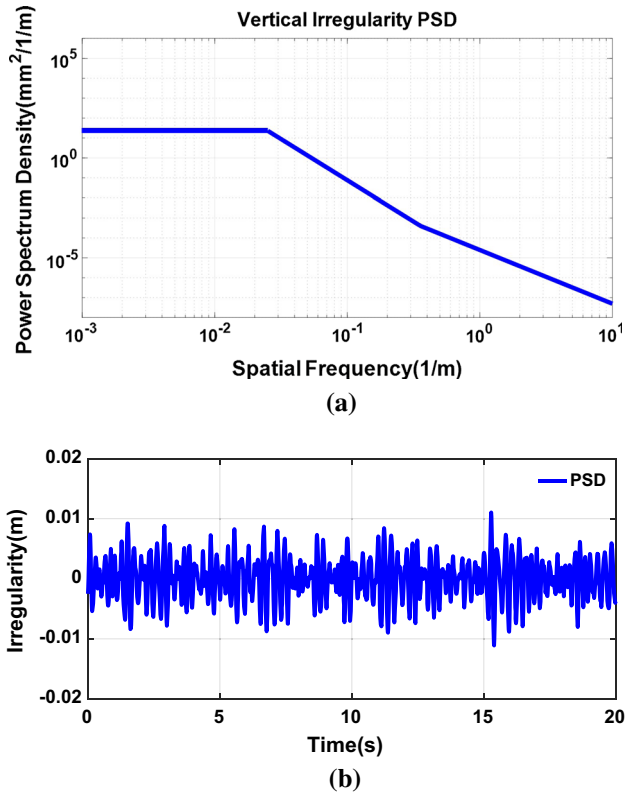

Fig. 5 Power spectral density (PSD) at 500 km/h: **a** spatial frequency; **b** irregularity

train bogie because they affect in vertical direction. They were located on the side of the bogie displacement. Input signals may be random or PSD-derived; random signaling assumes that the track has irregularities and PSD signaling is much more practical (Guangwei et al. 2007). Also, real trains are affected more largely by low-frequency disturbances because the resonance frequencies for the maglev exit mostly in the low frequency region. Figure 4 shows irregularities caused by random signaling. According to the references, the irregularity characteristics were defined as amplitude of about ± 0.01 m and the frequency range of about 0–50 Hz. Figure 4 was obtained by using MATLAB Simulink random signal function block. The random and PSD irregularities were applied in vertical direction and added as bogie levitation disturbances.

The PSD is as a function of the irregularities of a permanent maglev line (Shi et al. 2014). The PSD has been calculated by using the reference (Zhao and Zhai 2002). The data was based on Blackman-Tukey method using numerical time–frequency transfer method and discrete fast fourier transform (DFFT) methods. The speed of the data Fig. 5a shows the PSD spatial frequency. Figure 5b shows the irregularities of the PSD signals; PSD signals were also less than 0.01 m.

3 Simulation of dynamics of a maglev train

3.1 Construction of couple-fielded analysis

We employed MATLAB Simulink software controlled by the ADAMS subsystem in Fig. 6. Forces were entered using lookup tables and bogie displacements were then measured. Simulation was performed for 50 s after data were acquired over about 5 s, to ensure stability. The time step was 0.005 s. The ADAMS solver was written in C++ and the subsystem used non-linear analysis.

3.2 Dynamic simulation

In order to analyze the dynamic characteristics, the governing equations are required. However, it is too difficult to derive the governing equation for the full maglev system because they have many joints, 20th order modal information, and so on. So the multi-body commercial program (ADAMS^{TM}) was used instead of use of the governing

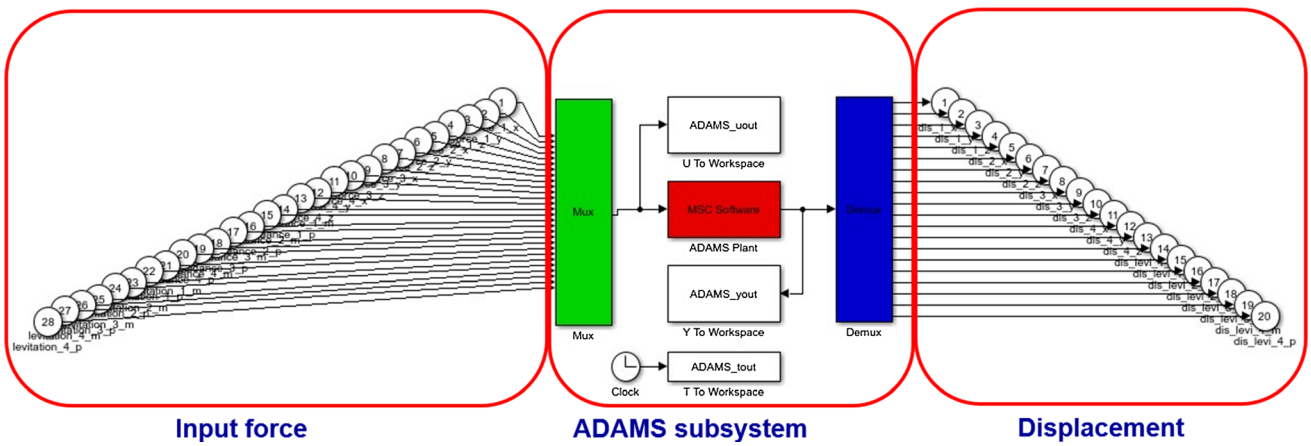

Fig. 6 ADAMS subsystem of MATLAB Simulink

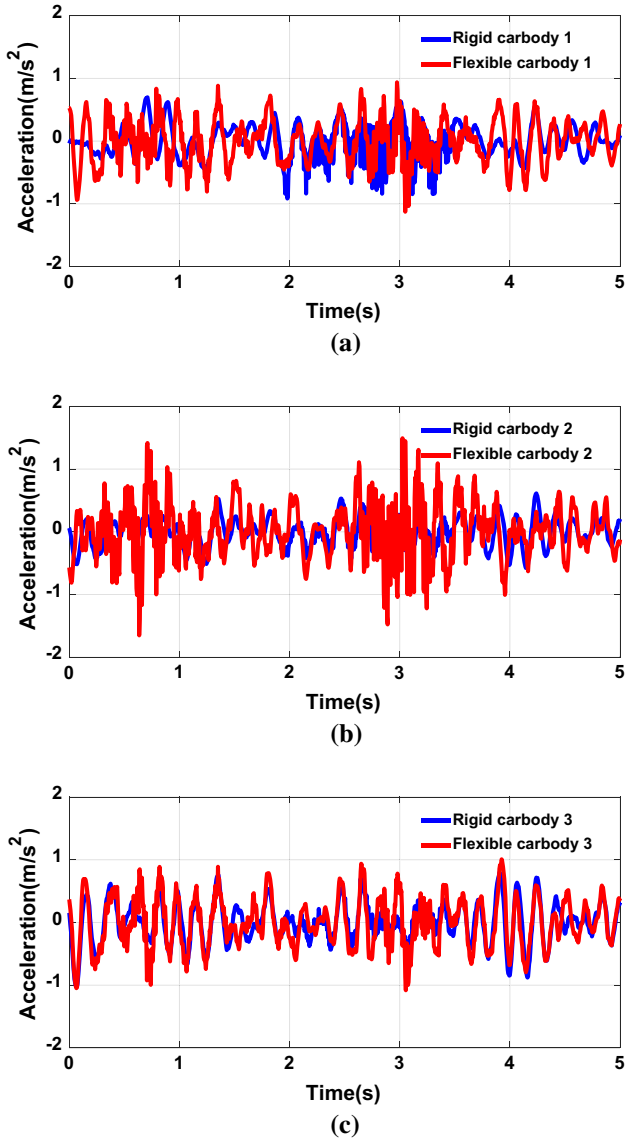

Fig. 7 Acceleration caused by random signals: **a** 1st car body; **b** 2nd car body; **c** 3rd car body

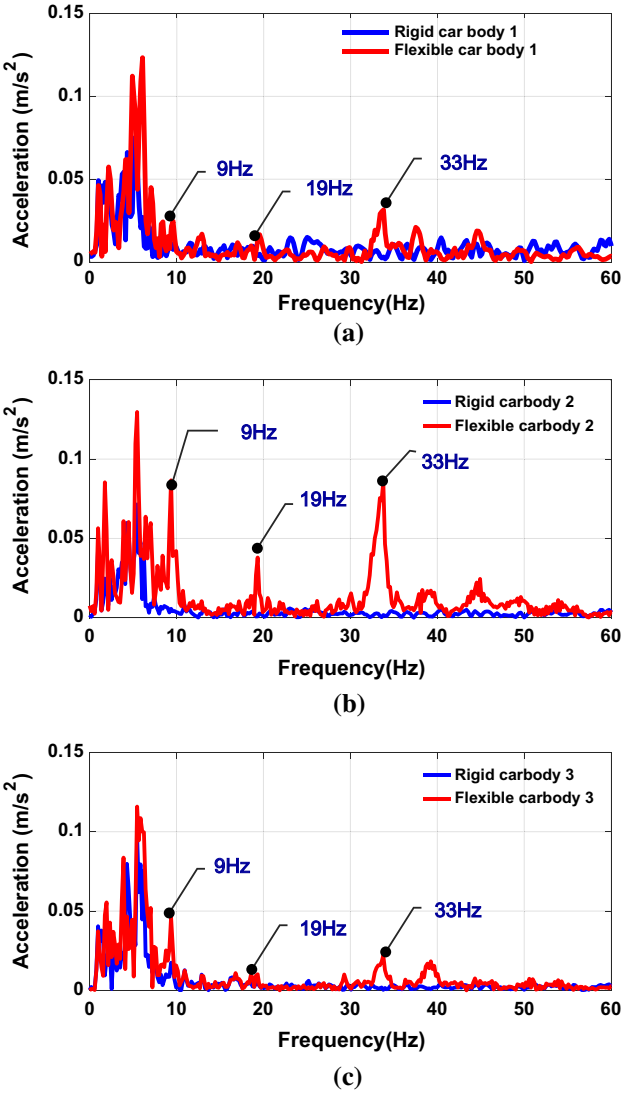

Fig. 8 Random signal acceleration FFT: **a** 1st car body; **b** 2nd car body; **c** 3rd car body

equation. Car body acceleration was measured at the center of mass (CM) point.

Figure 7 shows the simulation results using the frame work for constructed couple-fielded analysis. When a random signal was used as input irregularities, all car body accelerations were about 1 m/s^2. Car body vertical accelerations were based on peak-to-peak for all car bodies in time domain (Fig. 8).

The acceleration in Fig. 7b is greater than that in Fig. 7a, c. This is because although the input forces were identical, the 2nd car body was lighter than the 1st and 3rd car bodies. We used the FFT derived from the time history of random acceleration of Fig. 8a–c. The rigid body frequency was 1.5 Hz in the vertical mode, 3.7 Hz in the pitching mode, and 5.9 Hz in the rolling mode. The flexible car body modes are also shown in Fig. 8. The first bending frequency of the car bodies were 9 Hz. The second bending mode of the 1st and 3rd car bodies was 19 Hz. The middle-layer bending modes of the 1st and 3rd car bodies was 33 Hz. The articulated bogie was responsible for the 9 Hz peaks evident in Fig. 8a, c. As shown in Figs. 7 and 8, we found that a flexible car body acceleration was greater than a rigid acceleration because the elastic vibration modes which was excited by irregularities were added

Random car body displacements were measured peak-to-peak in vertical direction. Figure 9 shows the displacements measured at the CM point of the car body. Figure 9b shows that the flexible car body peak-to-peak displacements were larger than the rigid body displacements. Peak-to-peak vertical displacement for rigid car body was about 8.2 mm but, flexible car body peak-to-peak vertical

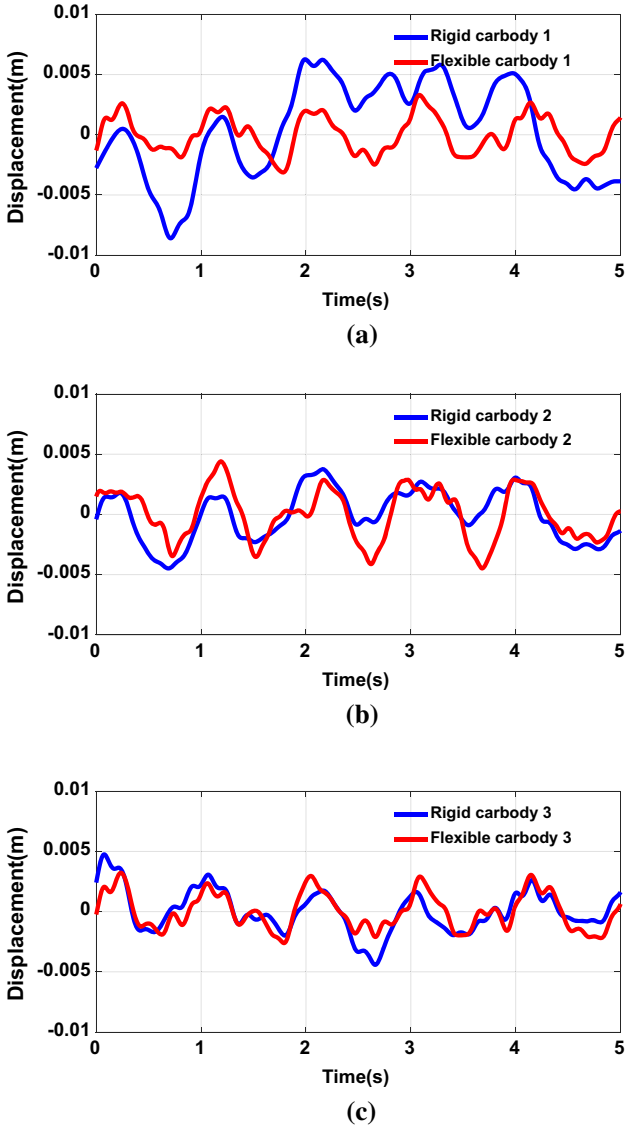

Fig. 9 Random signal displacements (rigid and flexible): **a** 1st car body; **b** 2nd car body; **c** 3rd car body

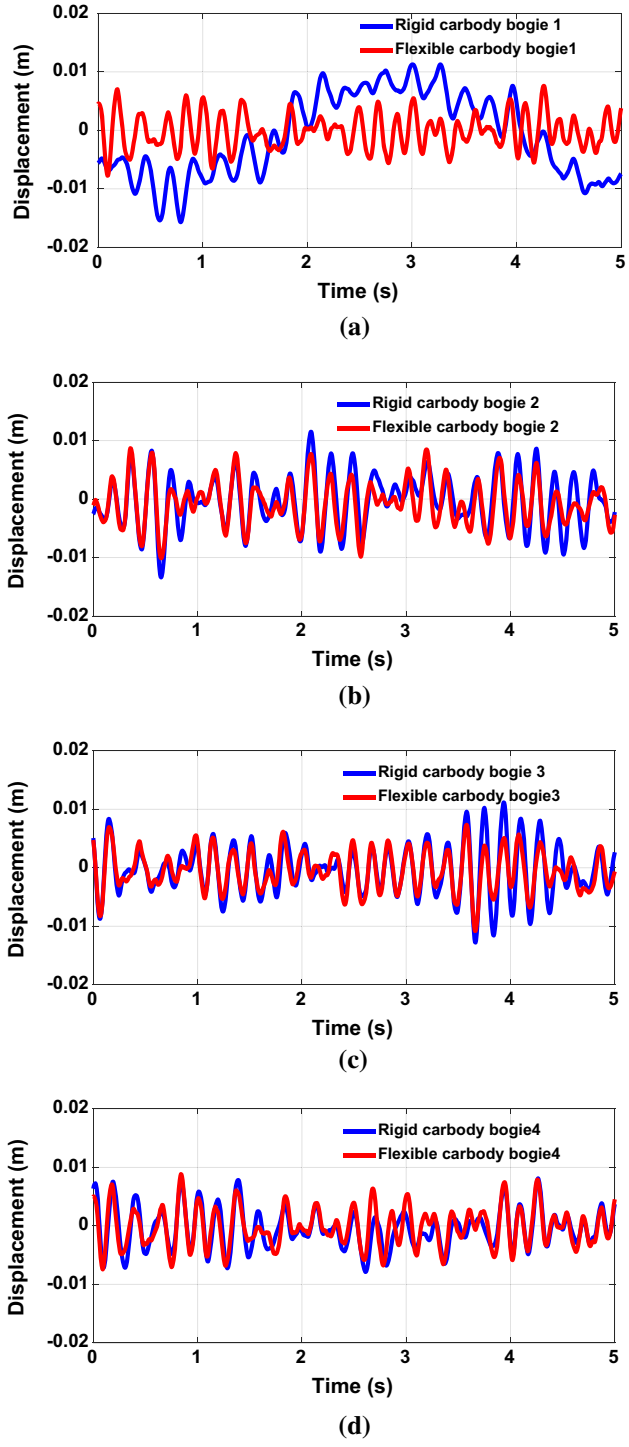

Fig. 10 Random signal displacements (rigid and flexible): **a** 1st; **b** 2nd; **c** 3rd; **d** 4th bogie

displacement was about 9 mm. Flexible car body has flexible modes but rigid car body doesn't have flexible modes. Therefore, flexible car body vibrates more than rigid car body modes. The 2nd car body weighed 23 tons and the 1st and 3rd are 32 tons. The peak-to-peak bogie vertical direction displacements, which were measured at CM point of the bogie are shown in Fig. 10. The 2nd and 3rd bogies were articulated, and thus were affected both the 2nd and 3rd car bodies. Also, action-reaction was in play when bogie vibration was high, such that car body vibration was also high.

The vibrational characteristics for PSD irregularities differed from those imparted by random signals, and were usually less than 0.01 m. The effect of PSD at 500 km/h on car body acceleration is shown in Fig. 11. Also, Fig. 11 shows the vertical acceleration measured in CM point on the car body. The PSD irregularities were larger than those of random signals. The PSD peak-to-peak maximum acceleration was about 3 m/s^2. Figure 11a–c show that the flexible car body acceleration was higher than the rigid acceleration because the flexible analysis considered the

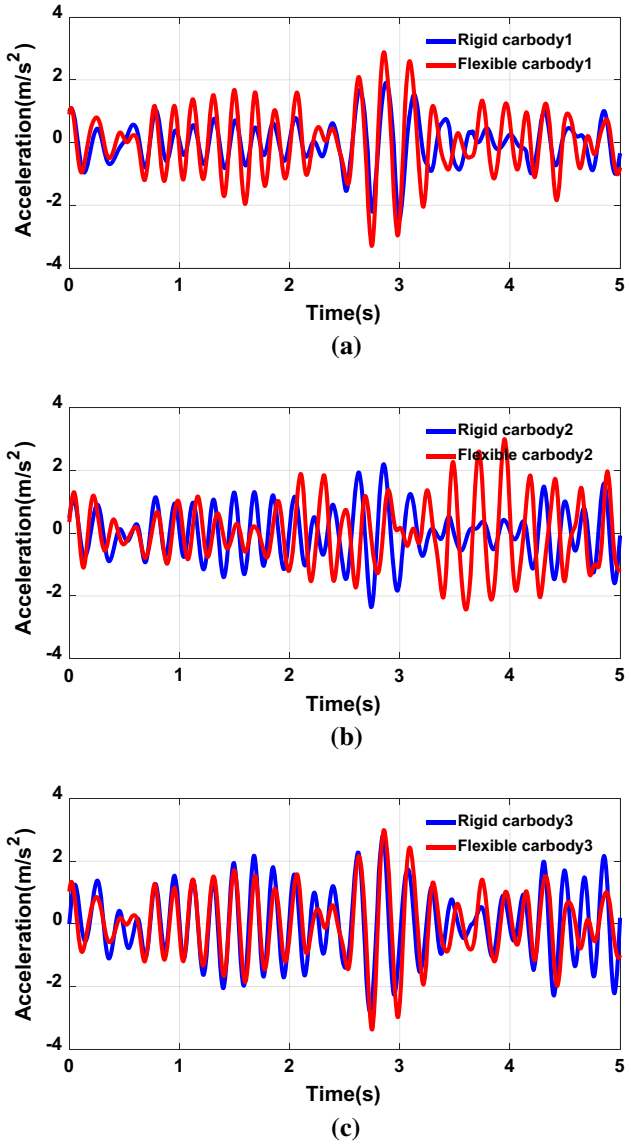

Fig. 11 PSD acceleration: **a** 1st car body; **b** 2nd car body; **c** 3rd car body

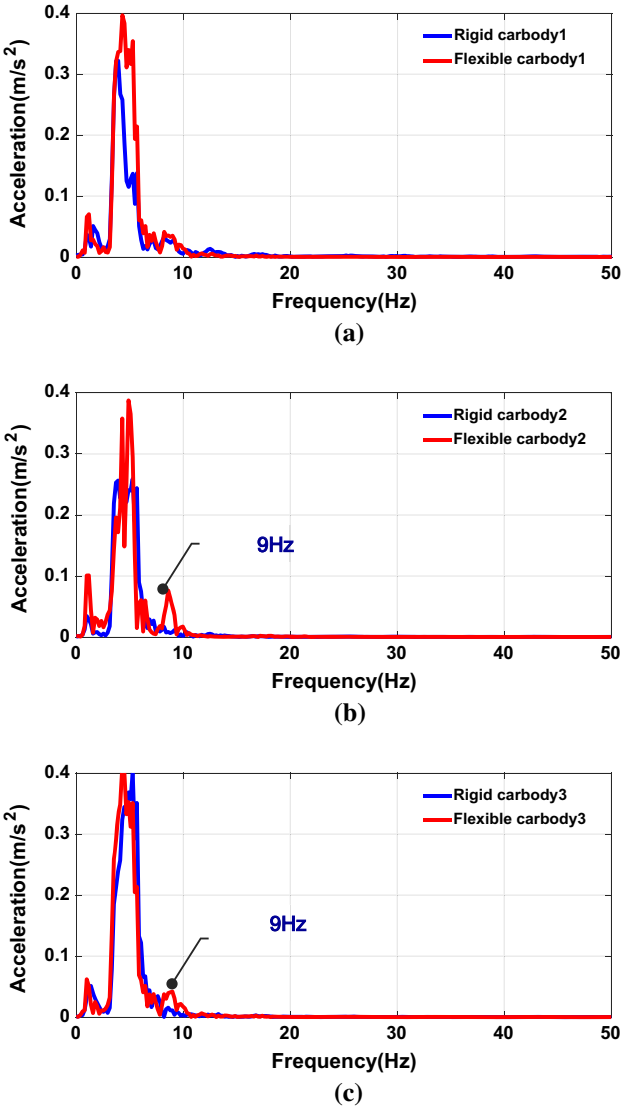

Fig. 12 PSD FFT acceleration: **a** 1st car body; **b** 2nd car body; **c** 3rd car body

vibrational modes and it included the effects. The acceleration data of Fig. 11 were subjected to FFT of Fig. 12. The rigid body frequencies were 1 Hz in the vertical mode and 5 Hz in the pitching mode. The PSD frequencies were all below 10 Hz. The first bending frequency is shown in Fig. 12b. The car bodies were articulated; the first bending mode of the 2nd car body affected that of the 3rd car body, as shown in Fig. 12c. When applying disturbance as a PSD in Fig. 12, PSD acceleration was twice bigger than applying random signal in Fig. 8 due to PSD's low frequency characteristics.

Figure 13 shows the vertical direction displacements measured on CM point of the car body for the rigid and flexible car body. The PSD displacements were twice as large as the random displacements because low-frequency disturbances affected the irregularities. The peak-to-peak displacement of rigid car bodies was about 10 mm and that of flexible car bodies was about 15 mm. Thus, use of the flexible mode increased displacement.

Figure 14 shows the vertical displacements of bogie which were measured at the CM point of the bogie. The PSD bogie displacements were also greater than the random displacements. Not only the car bodies, but also the bogies, were affected; the displacements doubled when PSD inputs were considered. Except for the 1st car body, the peak-to-peak displacements of the flexible car body models were larger than those of the rigid car body models, due to action-reaction. If a bogie exhibited large vibrations, the car body vibrates largely as well.

Except for the 1st car body, the PSD displacements were larger than the random displacements. Also, the 2nd and

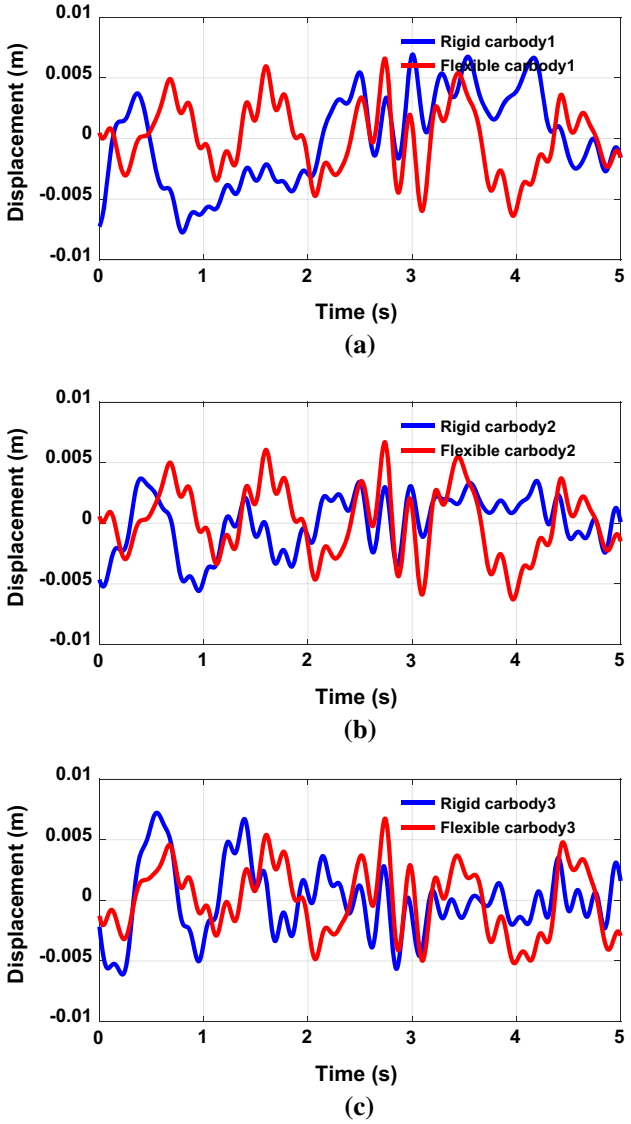

Fig. 13 PSD-triggered displacements (rigid and flexible): **a** 1st car body; **b** 2nd car body; **c** 3rd car body

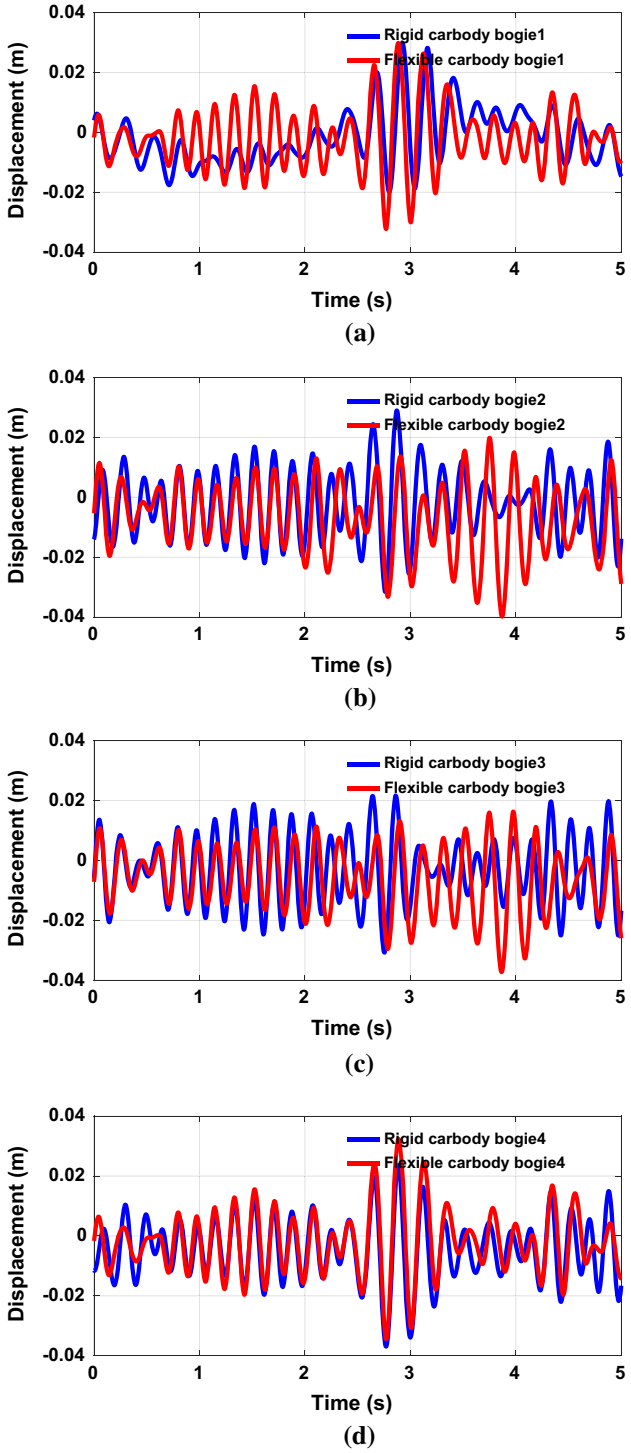

Fig. 14 PSD displacements (rigid and flexible): **a** 1st; **b** 2nd; **c** 3rd; **d** 4th bogie

3rd bogies vibrated more than did the 1st and 4th bogies due to action-reaction. The 2nd car body was affected by the 1st and 3rd car bodies because these latter bodies were articulated. The PSD-caused displacements were larger than the random displacements because the PSD acceleration was higher than the random acceleration attributable to the low-frequency characteristics of PSD acceleration; high-frequency modes were lacking. Table 1 shows the peak-to-peak vertical displacement which car body vibrates. The input of PSD signal car bodies and bogies vibrate about twice more than when applying random signal.

Table 2 shows ride comfort data based on KS R 9216, calculated using the random and PSD accelerations shown in Fig. 15. The flexible car body ride comfort data were poorer than those afforded using the rigid car body models, because flexible car body acceleration was greater than rigid car body acceleration. Car body acceleration affects ride comfort. Also, the PSD signal ride comfort was poorer than the random signal ride comfort for all car bodies. The

Table 1 Effects of random and PSD displacements

Car body model	Car body num.			Bogie num.			
Random signal displacement (mm)							
Rigid model	#1	#2	#3	#1	#2	#3	#4
Rigid model	14.8	8.2	6.1	26.7	25	24	16
Flexible model	#1	#2	#3	#1	#2	#3	#4
Flexible model	6.4	9.0	5.8	15.4	18.8	18.2	16.4
PSD signal displacement (mm)							
Rigid car body	#1	#2	#3	#1	#2	#3	#4
Rigid car body	14.1	9.4	8.4	49.6	56.4	52.6	50.0
Flexible car body	#1	#2	#3	#1	#2	#3	#4
Flexible car body	13.0	20	12.0	53.8	60.4	59.8	54.4

Table 2 Ride comfort associated with a random signal (rigid and flexible) and a PSD signal (rigid and flexible)

Car body model	Car body num.		
Random signal			
Rigid model	#1	#2	#3
Rigid model	107 dB	106 dB	109 dB
Flexible model	#1	#2	#3
Flexible model	110 dB	111 dB	111 dB
PSD signal			
Rigid model	#1	#2	#3
Rigid model	108 dB	109 dB	113 dB
Flexible model	#1	#2	#3
Flexible model	114 dB	112 dB	114 dB

random signal and PSD amplitudes were five-fold larger than the figures in Guangwei et al. (2007); the ride comfort level was thus about 100 dB. Accurate simulation requires analysis of PSD input to a flexible car body.

4 Conclusions

We simulated an EDS-type maglev train using multi-dynamic analysis, employing both rigid and flexible car body models. The flexible model featured vibrational modes, thus more closely approximating a real-world train. We used commercial software to create flexible car body models using the FEM method and converted the models to MNF files. We combined flexible car bodies with rigid bogies. ANSYS Maxwell software was used to calculate levitation and guidance forces, and a lookup table was created from which we input bogie forces. We then considered the irregularities of random and PSD signals. Random signals ranged over wide frequencies. However, PSD signals were all below 10 Hz, thus very similar to real-world irregularities. The effect of PSD inputs on bogie displacement was greater than that of random signal inputs. The 2nd and 3rd bogies vibrated more than the 1st and 4th bogies due to action-reaction. The body mass differed among the car bodies; the 2nd car body vibrated more than did the 1st and 3rd car bodies. Also, the 2nd car body exhibited flexible vibrational modes on both random and

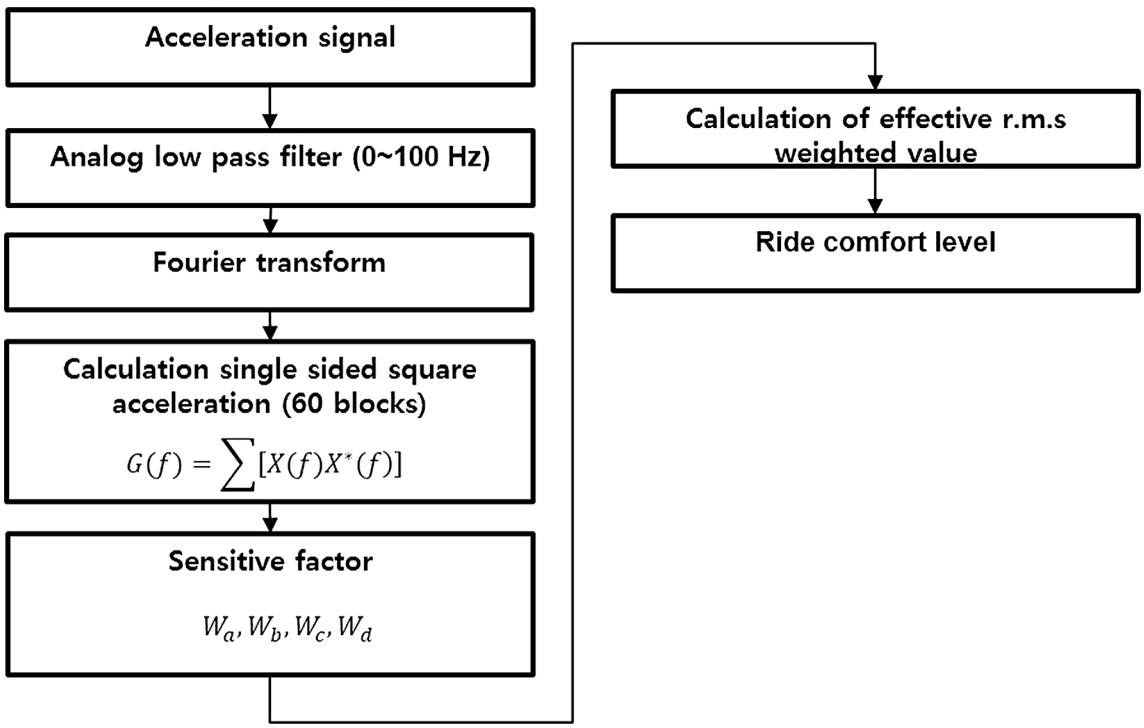

Fig. 15 Calculation method of ride comfort

PSD signal input. The flexible model of the 2nd car body affected the 3rd car body because the bogies were articulated. Next, we simulated acceleration to calculate ride comfort, which was poorest when PSD signals were input and best when random signals were delivered (rigid model). The use of PSD inputs and flexible car body models improved the simulation accuracy.

Acknowledgements This work was supported by the Gachon University research fund of 2018. (GCU-2018-0318) and from Human Resource Development of the Korea Institute of Energy Technology Evaluation and Planning (KETEP) and the Ministry of Trade, Industry and Energy (MOTIE) of the Republic of Korea (20174030201530).

References

Ahmed R, Jun YL, Azhar MF, Junejo NUR (2014) Comprehensive study and review on maglev train system. Appl Mech Mater 615:347–351

Diana G, Cheli F, Collina A, Corradi R, Melzi S (2002) The development of a numerical model for railway vehicles comfort assessment through comparison with experimental measurements. Veh Syst Dyn 38(3):165–183

Early R, Yoshitomo A, Hiroyuki O (2002) Numerical analysis of the vehicle dynamics of the superconducting maglev system at the Yamanashi test line. In: The 17th international conference on magnetically levitated systems and linear drives (Maglev 2002), Lausanne, 3–5 September 2002

Fujie J (1999) An advanced arrangement of the combined propulsion, levitation and guidance system of superconducting Maglev. IEEE Trans Magn 35(5):4049–4051

Fujimoto T, Aiba M, Suzuki H, Umeki T, Nakamura S (2000) Characteristics of electromagnetic force of ground coil for levitation and guidance at the Yamanashi Maglev test line. Q Rep RTRI 41(2):63–67

Guangwei S, Meisinger I R, Gang S (2007) Modeling and simulation of Shanghai maglev train transrapid with random track irregularities. Sonderdruck Schriftenreihe der Georg-Simon-Ohm-FachhochschuleNürnberg 39:11S

Hoshino H, Suzuki E, Watanabe K (2008) Reduction of vibrations in Maglev vehicles using active primary and secondary suspension control. Q Rep RTRI 49(2):113–118

Hoshino H, Suzuki E, Yonezu T, Watanabe K (2012) Examination of vehicle motion characteristics of a Maglev train set using a reduced-scale model experiment apparatus. Q Rep RTRI 53(1):52–58

Kim IK, Kratz R, Doll D (2002) Technology development for US Urban Maglev. In: Maglev 2002 conference, Lusanne, Switzerland

Kim D, Park N, Yoo J, Lim S (2018) Transient EM force estimation for EDS type maglev using 3D FE model. In: Proceedings of the Maglev 2018 conference

Lee HW, Kim KC, Lee J (2006) Review of maglev train technologies. IEEE Trans Magn 42(7):1917–1925

Miyamoto S, Osada Y, Katsumi Y, Tsutomu F (2004) The Status of the running tests of JR-Maglev. Maglev 1:60–64

Ohsaki H, Bando S (2006) Numerical analysis of elastic vibration of superconducting maglev vehicles. In: MAGLEV'2006: the 19th international conference on magnetically levitated systems and linear drives transrapid International GmbH und company KGMaxBoglBauunternehmung GmbH und Company KGDeutsche Bahn AGIABG mbHNexans Deutschland GmbHDornier Consulting GmbH

Ohsaki H, Early RW, Suzuki E (2000) Numerical simulation of the vehicle dynamics of the superconducting maglev system. In: The 16th international conference on magnetically levitated systems and linear drives, Rio de Janeiro, pp 230–235

Rose CR, Peterson DE, Leung EM (2008) Implementation of Cargo MagLev in the United States. URL: http://www.researchgate.net/publication/228994479_Implementation_of_cargo_MagLev_in_the_United_States. Accessed 25 May 2017

Seki A, Osada Y, Kitano JI, Miyamoto S (1996) Dynamics of the bogie of a maglev system with guideway irregularities. IEEE Trans Magn 32(5):5043–5045

Shi J, Fang WS, Wang YJ, Zhao Y (2014) Measurements and analysis of track irregularities on high speed maglev lines. J Zhejiang Univ Sci A 15(6):385–394

Shirakuni N, Endo Y, Takahashi K, Yamamoto K (2002) Overview of new vehicles for the Yamanashi Maglev Test Line. In: Proceedings of the 17th international conference on magnetically levitated systems (Maglev 2002)

Song MK, Fujino Y (2008) Dynamic analysis of guideway structures by considering ultra high-speed Maglev train-guideway interaction. Struct Eng Mech 29(4):355–380

Suzuki E, Shirasaki J, Watanabe K, Hoshino H, Nagai M (2008) Comparison of methods to reduce vibrations in superconducting maglev vehicles by primary suspension control. J Mech Syst Transp Logist 1(1):3–13

Tanaka M, Aiba M, Suzuki M (2007) Development of electromagnetic vibration test apparatus for ground coils applied to maglev system. Q Rep RTRI 48(2):110–114

Tomioka T, Suzuki Y, Takigami T (2003) Three-dimensional flexural vibration of lightweight railway vehicle carbody and a new analytical method for flexural vibration. Q Rep RTRI 44(1):15–21

Tsuruga H (1992) Superconductive maglev system on the Yamanashi maglev test line. SAE Trans 101:196–201

Yaghoubi H, Ziari H (2010) Development of a maglev vehicle/guideway system interaction model and comparison of the guideway structural analysis with railway bridge structures. J Transp Eng 137(2):140–154

Yamamoto K, Kozuma Y, Tagawa N, Hosaka S, Tsunoda H (2004) Improving maglev vehicle characteristics for the Yamanashi test line. Q Rep RTRI 45(1):7–12

Yonezu T, Watanabe K, Suzuki E, Sasakawa T (2017) Study on electromagnetic force characteristics acting on levitation/guidance coils of a superconducting Maglev vehicle system. IEEE Trans Magn 53(11):1–5

Zhang YW, Zhao Y, Zhang YH, Lin JH, He XW (2013) Riding comfort optimization of railway trains based on pseudo-excitation method and symplectic method. J Sound Vib 332(21):5255–5270

Zhao CF, Zhai WM (2002) Maglev vehicle/guideway vertical random response and ride quality. Veh Syst Dyn 38(3):185–210

Zhou J, Goodall R, Ren L, Zhang H (2009) Influences of car body vertical flexibility on ride quality of passenger railway vehicles. Proc Inst Mech Eng Part F J Rail Rapid Transit 223(5):461–471